Earth and Space Science

RESEARCH ARTICLE
10.1029/2019EA000911

First Observation of Ionospheric Convection From the Jiamusi HF Radar During a Strong Geomagnetic Storm

J. J. Zhang[1], W. Wang[1], C. Wang[1], A. L. Lan[2], J. Y. Yan[2], D. Xiang[2], Q. H. Zhang[3], J. M. Ruohoniemi[4], B. S. R. Kunduri[4], N. Nishitani[5], X. Shi[4], and H. B. Qiu[6]

[1]State Key Laboratory of Space Weather, National Space Science Center, Chinese Academy of Sciences, Beijing, China, [2]Key Laboratory of Microwave Remote Sensing, National space Science Center, Chinese Academy of Sciences, Beijing, China, [3]Shandong Provincial Key Laboratory of Optical Astronomy and Solar-Terrestrial Environment, Institute of Space Sciences, Shandong University, Weihai, China, [4]Center for Space Science and Engineering Research (Space@VT), Virginia Polytechnic Institute and State University, Blacksburg, VA, USA, [5]Institute for Space-Earth Environmental Research, Nagoya University, Nagoya, Japan, [6]Jiamusi University, Jiamusi, China

Key Points:
- A new middle-latitude HF coherent scatter radar was deployed in Jiamusi, China
- The first observation of the ionospheric convection from the radar during a strong storm is presented and validated
- The inclusion of the data into calculation of SuperDARN convection increases the cross-polar cap potential

Correspondence to:
J. J. Zhang,
jjzhang@spaceweather.ac.cn

Citation:
Zhang, J. J., Wang, W., Wang, C., Lan, A. L., Yan, J. Y., Xiang, D. et al. (2020). First observation of ionospheric convection from the Jiamusi HF radar during a strong geomagnetic storm. *Earth and Space Science*, 7, e2019EA000911. https://doi.org/10.1029/2019EA000911

Received 26 SEP 2019
Accepted 18 NOV 2019
Accepted article online 11 DEC 2019

Abstract The Super Dual Auroral Radar Network (SuperDARN) is an international low-power high-frequency (HF) radar network, which provides continuous observations of the motion of plasma in the ionosphere. Over the past 15 years, the network has expanded dramatically in the middle latitudes of the Northern Hemisphere to improve the observation capabilities of the network during periods of strong geomagnetic disturbance. However, a large coverage gap still exists in the middle latitudes. A newly deployed middle-latitude HF radar in China (the Jiamusi radar) is about to join the network. This paper presents the first observation of the ionospheric convection from the Jiamusi radar during the strong geomagnetic storm on 26 August 2018. The Jiamusi measurements are compared with the simultaneous measurements from the SuperDARN Hokkaido East radar. The features of the high-velocity westward flows including the equatorward expansion and variation tendency of the line-of-sight velocities observed by the two radars are consistent with each other. According to joint analysis with auroral images, we can confirm that the westward flows observed by the two radars are sunward return flows of the duskside convection cell in the auroral region. The impact the Jiamusi data had on the calculation of SuperDARN convection patterns is also examined. The results show that the inclusion of the Jiamusi data can increase the number of gridded line-of-sight velocity measurements by up to 24.42%, the cross-polar cap potential can be increased by up to 13.90% during the investigated period.

1. Introduction

Solar wind drives the circulation of plasma in the magnetosphere primarily by the magnetic reconnection process at the dayside magnetopause and in the nightside magnetotail (Dungey, 1961). In addition, viscous-like interactions between the magnetosphere and solar wind also play a role in this momentum transfer process (Axford & Hines, 1961; Kivelson & Russell, 1995). High-latitude ionospheric convection in the Earth is coupled tightly to the circulation of plasma in the magnetosphere via magnetic field lines. For southward interplanetary magnetic field (IMF) conditions, the ionospheric convection conforms to a classical two-cell pattern with antisunward cross-polar cap flow from noon to midnight and sunward return flow at lower latitudes along the dusk and dawn flank in the auroral regions. Under northward IMF conditions, the convection weakens and reversed convection cells can be observed on the dayside polar cap, which is due to the reconnections occurring at the lobe cell of the magnetosphere leading sunward flows on the polar cap (Crooker, 1992). The ionospheric convection pattern is very useful in studies of the solar wind and magnetosphere-ionosphere (M-I) coupling system. It plays an important role in measuring the energy transfer from the solar wind into the magnetosphere and ionosphere system (Pettigrew et al., 2010). Statistical convection models have been derived by using a variety of data sets and techniques, such as measurements from the Defense Meteorological Satellite Program (DMSP) satellites (Rich & Hairston, 1994), Dynamics Explorer spacecraft (Weimer, 1995, 1996), ground-based magnetometers (Friis-Christensen et al., 1985; Richmond & Kamide, 1988), incoherent scatter radars (Foster, 1983), and high-frequency (HF) coherent scatter radars (Ruohoniemi & Greenwald, 1996, 2005; Thomas & Shepherd, 2018) as well.

Figure 1. A bird's eye view of the Jiamusi radar site taken by a small unmanned aerial vehicle with the main antenna array across the picture from the bottom left to the top right, the interferometric array pictured in the upper left, and the equipment shelter with the blue roof located between the two antenna arrays.

The network of HF coherent scatter radars that is well known as the Super Dual Auroral Radar Network (SuperDARN) has been a very important tool in studying ionospheric convection and the M-I coupling process. Especially, it has the ability of studying the global-scale dynamics of plasma convection in the high-latitude ionosphere (Chisham et al., 2007; Zhang et al., 2013). The SuperDARN radars were built at high latitude and polar region (above geomagnetic latitude [MLAT] 55°); at first, this was enough to obtain the ionospheric patterns for typical conditions. However, during geomagnetically active periods when the auroral region expands lower than the lower-latitude limit of the existing network, the limitation of the high-latitude network arises at measuring the full spatial extent of the high-latitude ionospheric convection. Under these circumstances, the cross-polar cap potential (Φ_{pc}) obtained from the models based on the SuperDARN data tends to be weaker than that from the others (Baker et al., 2007). To overcome this shortcoming, the network needed to expand to lower latitudes. The first middle-latitude HF radar, which is located on Wallops Island (WAL), Virginia, became operational in 2005. A study by Baker et al. (2007) indicated that the Wallops radar captured the expansion of auroral electric fields to middle latitudes during disturbed geomagnetic conditions ($Kp \geq 3$), and the average SuperDARN cross-polar cap potential was increased by 25% by incorporating the Wallops radar measurements into the calculation of convection pattern. From then on, the middle-latitude SuperDARN radar network has been greatly developed. As of 1 January 2018, there were a total of 10 middle-latitude radars in the Northern Hemisphere stretching from eastern United States to Japan. Thomas and Shepherd (2018) produced a statistical model of ionospheric convection by using line-of-sight (LOS) velocity data from all available SuperDARN radars. They found that Φ_{pc} can be increased by as much as 40% by including the 10 middle-latitude radars data in the model.

Over the past 15 years of operating middle-latitude SuperDARN radars, many accomplishments have been achieved (Nishitani et al., 2019). However, the expansion of middle-latitude radars is far from being complete; there is still a large coverage gap region existing that stretches from eastern Asia to Europe. More radars need to be built in this region. A new middle-latitude HF coherent scatter radar has been constructed in Jiamusi, China, and is currently in full operation. This paper presents the first observation of ionospheric convection from the Jiamusi radar (JME) during a strong geomagnetic storm and shows how the data contribute to the whole convection pattern based on SuperDARN data. In section 2, we give a brief description of the Jiamusi radar, especially, the innovations in design of the radar system. In section 3, we present the observations of the Jiamusi radar during the strong storm on 26 August 2018 and compare the measurements with the SuperDARN Hokkaido East radar (HOK); then we present and discuss the contribution of the Jiamusi radar data to the convection patterns in the Northern Hemisphere during the storm. A brief summary and conclusion are given in the final section of the paper.

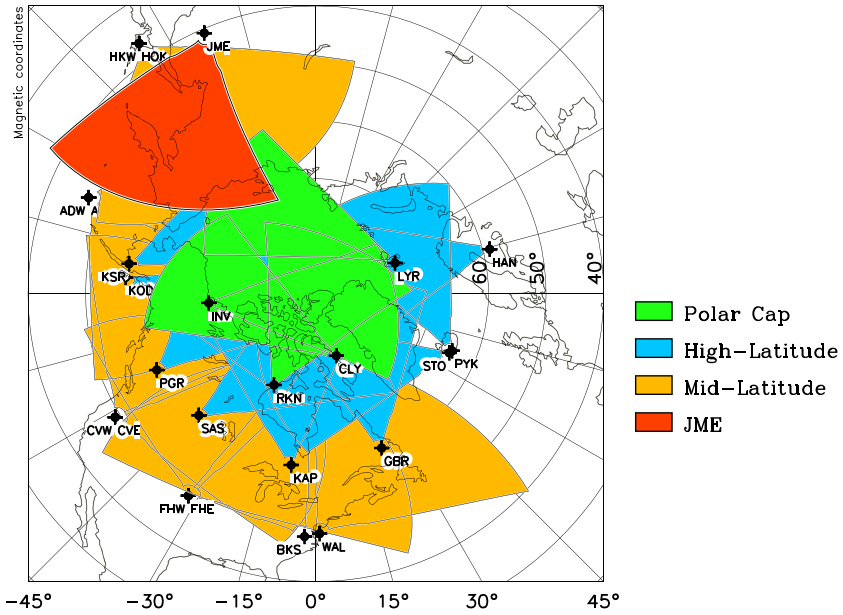

Figure 2. The FOV of the Jiamusi radar along with the other Northern Hemisphere SuperDARN radars in operation. The FOV for the Jiamusi radar is shaded red, and the FOVs for the other middle-latitude, high-latitude, and polar cap radars are shaded yellow, blue, and green, respectively. The FOVs are plotted in geomagnetic coordinates.

2. The Jiamusi Radar

The Jiamusi radar was developed by the National Space Science Center, Chinese Academy of Science. It is deployed in Changfa town, Jiamusi city, China. The geographic coordinates of the radar site are 46.8°N, 130.5°E (41.8°N,155.1°W in Altitude Adjusted Corrected Geomagnetic magnetic coordinates). It looks to the northeast with a boresight azimuth of 44° in geographic coordinates. Designed as a kind of SuperDARN radar, it follows the basic design principles of SuperDARN radars. Compared with most existing SuperDARN radars, the notable innovation in the Jiamusi radar is the application of the Field Programmable Gate Array-based digital beam forming (DBF) technique in hardware design of the radar system. The application of the DBF technique allows much more flexible beam direction steering than the previous time delay steering. To achieve the required DBF accuracy, real-time internal calibration is carried out to keep the transmitter/receivers phase consistency. Just as the middle-latitude SuperDARN radars deployed in the Unites States, Jiamusi radar utilized the twin-terminated folded dipole antenna with corner reflector (Sterne et al., 2011). The antenna array consists of a main array of 16 elements and an interferometric array of 4 elements. A bird's eye view of the radar site taken by a small unmanned aerial vehicle is shown in Figure 1, with the main antenna array across the picture from the bottom left to the top right, the interferometric array pictured in the upper left, and the equipment shelter with the blue roof located between the two antenna arrays.

The radar scans over 78° of azimuth in 24 beam directions separated by 3.25°, with 75 range gates along each beam separated by 45 km. The fields of view (FOVs) of the Jiamusi radar along with the other Northern Hemisphere SuperDARN radars in operation are plotted in geomagnetic coordinates and shown in Figure 2. The FOV for the Jiamusi radar is shaded red, and the FOVs for the other middle-latitude, high-latitude, and polar cap radars are shaded yellow, blue, and green, respectively. According to the figure, we can see that the Jiamusi radar has a common viewing area with the Hokkaido pair of radars (HOK and HKW), which would provide a two-dimensional observation of ionospheric convection in this area. The first-light data of the Jiamusi radar was received in January 2018. The radar experienced its first strong geomagnetic storm on 26 August 2018.

3. Results

In this section, we present a description of IMF and solar wind conditions and SYM-H index during the strong geomagnetic storm of 26 August 2018 (section 3.1). Observations from the Jiamusi radar during 0400 to 0800 UT are presented and compared with the simultaneous observations obtained by the Hokkaido East

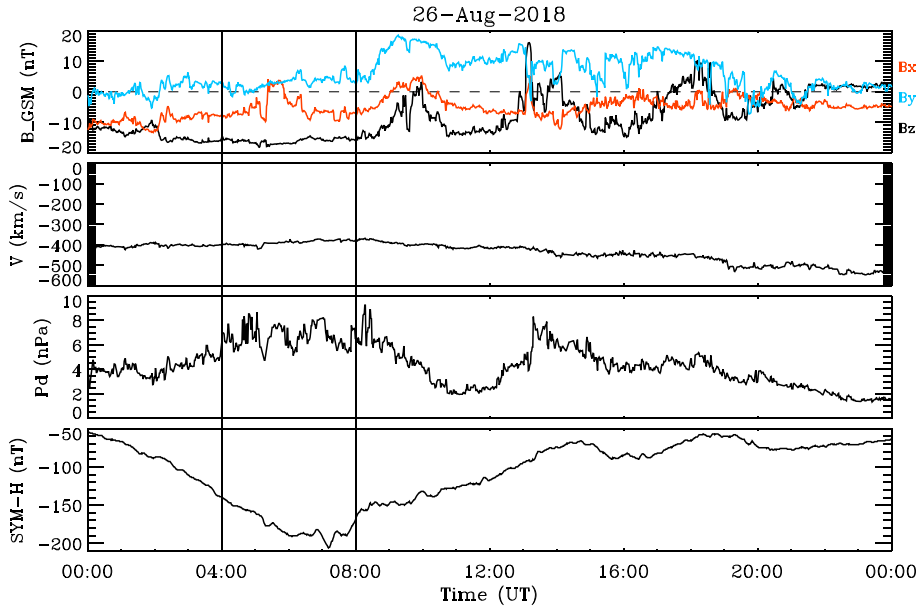

Figure 3. The time series of the IMF and solar wind parameters as well as the SYM-H index on 26 August 2018. The parameters from top to bottom are three components of the IMF, *x* component of solar wind velocity, solar wind dynamic pressure, and the SYM-H index. The two vertical lines indicate the time interval of 0400 UT to 0800 UT.

radar to validate the Jiamusi data. The auroral images obtained from the Special Sensor Ultraviolet Spectrographic Imager (SSUSI) on board the DMSP satellites and the observations from the two radars (JME and HOK) are overlapped together when the satellites flew cross the Northern Hemisphere. The motivation is to identify what type of ionospheric flows the radar observed. Were they the auroral region sunward return flows of the Dungey circle or the subauroral polarization streams (section 3.2)? We also examined the effect that the Jiamusi data have on the calculation of the SuperDARN convection patterns during this event. Variations of the number of data points go into the convection calculation model and variations of the cross-polar cap potential after incorporating the Jiamusi radar observation into the calculation of the convection pattern are presented to provide a quantitative measure of the effect (section 3.3).

3.1. The Strong Storm of 26 August 2018

Figure 3 shows the time series of the IMF and solar wind parameters as well as the SYM-H index on 26 August 2018 obtained from the OMNI database on the CDAweb (https://omniweb.gsfc.nasa.gov/ow.html). The parameters from top to bottom are three components of the IMF, *x* component of solar wind velocity, solar wind dynamic pressure, and the SYM-H index. The two vertical lines in the figure indicate the time interval of interest for the radar measurements (0400–0800 UT). The IMF B_z component remained on a strong southward orientation for more than 8 hr followed by several dramatic direction reversals and finally returned to a weak northward orientation by the end of the day. Solar wind velocity kept at approximately −400 km/s most of the time and increased gently after 1200 UT, while dynamic pressure underwent drastic variations during the day. The SYM-H index went down from −55 nT at the beginning of the day to its minimum −206 nT at 0711 UT, and then it started to recover. The NOAA Space Weather Prediction Center classified this storm as a strong G3 geomagnetic storm. Caused by a weak coronal mass ejection during solar minimum, the unexpected strong geomagnetic storm was attributed to the enhanced magnetic field with a persistent southward IMF B_z (Chen et al., 2019).

3.2. Radar Observation

The Jiamusi radar observed high-velocity flows moving toward the radar with maximum LOS velocity exceeded 1,000 m/s during the main phase of the storm. Figure 4 shows the time series plots of the measurements from Beam 6 of the Jiamusi radar obtained between 0400 and 0800 UT on 26 August 2018. The beam direction is aligned east of the magnetic north (see Figure 5). Figure 5 shows the FOVs of the Jiamusi radar and the Hokkaido east radar HOK; Beam 6 of each radar is highlighted in black. Measurements from Beam 6 of these two radars will be compared then. The parameters of backscatter power, LOS Doppler velocity, and spectral width are shown in Figure 4 from the top panel to the bottom panel. They are plotted versus

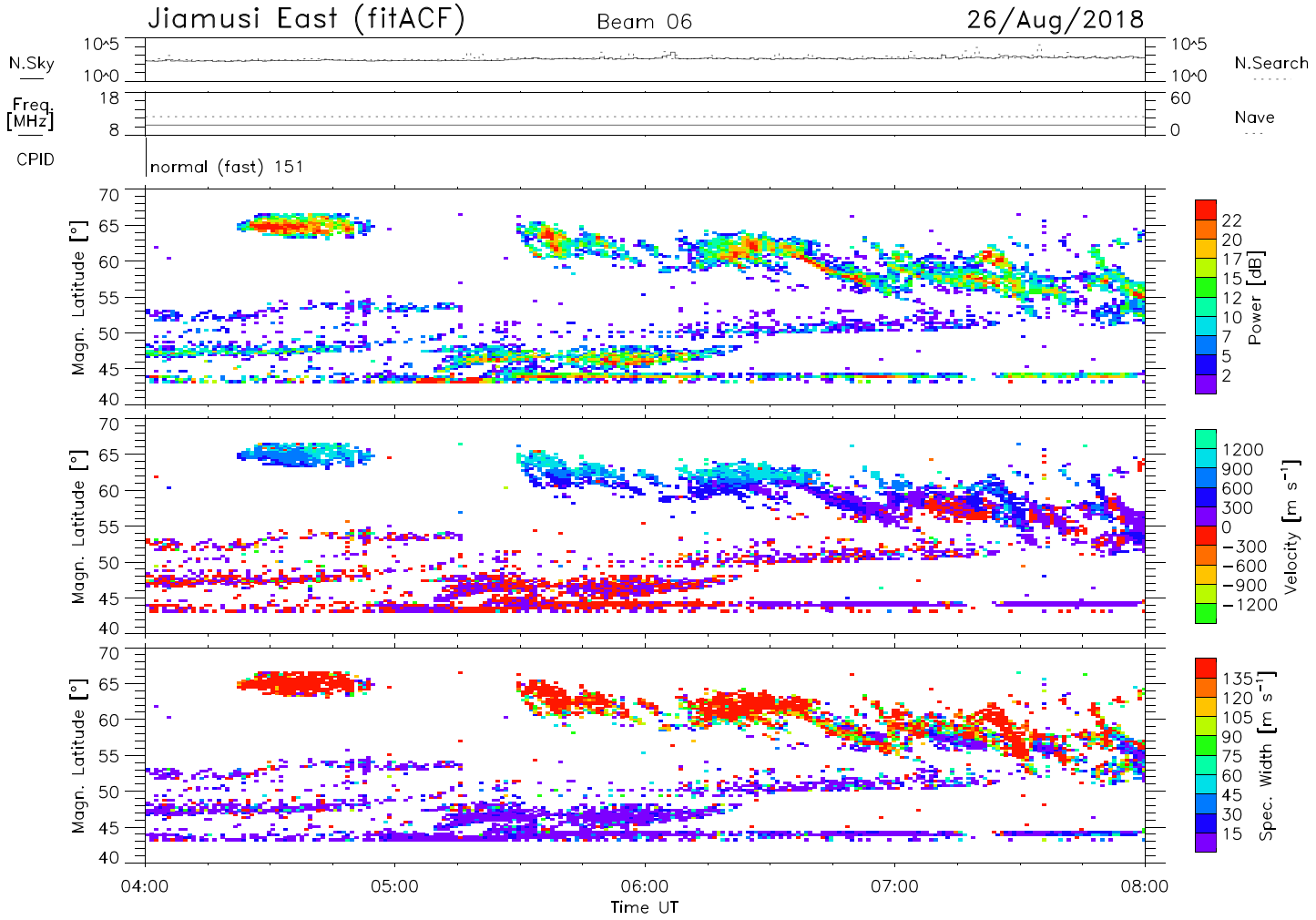

Figure 4. The time series plots of measurements from Beam 6 of the Jiamusi radar obtained between 0400 and 0800 UT on 26 August 2018. At the top of the figure are the receiver noise and transmitted frequency. The parameters of backscatter power, LOS Doppler velocity, and spectral width are shown from the top panel to the bottom panel. Each parameter is color coded according to the color bar on the right.

magnetic latitude. Each parameter is scaled according to the color bar on the right. In the middle panel, the negative LOS Doppler velocities represent plasma flows away from the radar, while the positive represent plasma flows toward the radar. At the top of the figure are the receiver noise and transmitted frequency. The operating frequency was kept at 10.4 MHz during this day. On this day the Jiamusi radar was operating in normal (fast) mode; it scans counterclockwise with each scan commencing on a 1-min boundary. During this period, the low-velocity scatters distributed below 55° are mostly ground scatters. Besides, at the nearest range gates the scatters are mostly *E* region echoes or scatters from meteor trails (Baker et al., 2007). These scatters are not taken into account when discussing *F* region plasma convection. Starting at 0422 UT, the Jiamusi radar began to observe strong positive ionospheric velocities forming in a well-defined region centered at ~65° geomagnetic latitude. The velocities increased with time and reached the maximum at around 0445 UT and then decreased slightly until the ionospheric scatters disappeared at approximately 0455 UT on this beam. The ionospheric scatters with high positive LOS velocities jumped out again at 0530 UT. From 0640 UT the ionospheric scatters became distributed in a wider range and the LOS velocities dropped to a lower level. From 0422 to 0800 UT the overall trend of the ionospheric scatter was to move equatorward to lower magnetic latitudes. As was stated by Baker et al. (2007) when they interpreted the equatorward movement of the ionospheric scatter observed by the Wallops radar during a storm, this trend can be attributed to two reasons: (1) the latitude of the auroral oval varies with local time and (2) auroral zone extended equatorward as the development of the geomagnetic storm during main phase.

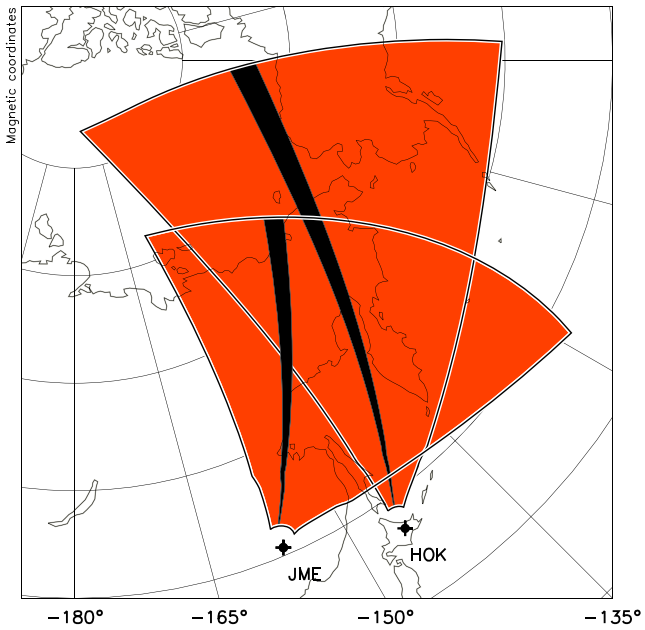

Figure 5. The FOVs of the Jiamusi radar and the Hokkaido east radar; Beam 6 of each radar is highlighted in black.

To validate the measurements of the Jiamusi radar, the LOS velocities measured from Beam 6 of the Jiamusi radar are compared with those from Beam 6 of the Hokkaido East radar. The direction of the two beams can be seen in Figure 5. The range of the Jiamusi radar was set to 75 range gate during that period; the number of beam was 24. While the range of the Hokkaido East radar was 110 range gate, the number of beam was 16. The Jiamusi radar operated in fast normal mode during that day, which means the time resolution of the data on each beam was 1 min. The Hokkaido East radar operated in RBSP mode that day; time resolution of the data for three beams (Beams No.0, No.1, and No.3) was 20 s, which was approximately 2 min for the other beams. Figure 6 shows time series plots of observations from the Beam 6 of the Jiamusi radar (Figure 6a) and the Hokkaido East radar (Figure 6b) between 0400 and 0800 UT on 26 August 2018. The LOS velocities are color coded according to the color bar on the right; the ground scatters are marked gray in this figure. According to the measurements from all the beams of the two radars, the observed high-velocity flows were mostly westward. From the figure, it can be seen that the center latitude of the region of westward flows observed by the Jiamusi radar moved from ~65° at 0422 UT to 56° at 0800 UT. The westward flows observed by Beam 6 of the Hokkaido East radar shifted from ~66° at 0400 UT to 58° at about 0730 UT. The maximum magnitude of the LOS velocities reached to ~1,000 m/s during the period and decreased to a lower value at 0730 UT. Both of the two beams observed the similar feature of the equatorward extension of the westward flows during the storm's main phase. And the LOS velocities observed by the two radars were comparable.

Comprehensive analysis of measurements of auroral activity and ionospheric convection is necessary to identify the convection features. With the information of the equatorward edge of the auroral oval, the auroral region convection and subauroral polarization stream can be distinguished. The SSUSI instrument onboard DMSP is a hyperspectral cross-track scanning spectrometer that measures auroral emission at five far-ultraviolet spectral bins: N_2 LBHS (140–152 nm), LBHL (164–180 nm), O (130.4 nm), O (135.6 nm), and H (121.6 nm) (Sotirelis et al., 2013). Electron aurora (135.6-nm atomic oxygen line) provided by SSUSI are used in this study. We examined the observations by the Jiamusi radar and the Hokkaido East radar during 0400 to 00800 UT when the DMSP satellites passed over. The westward flows observed by the Jiamusi radar and the Hokkaido East radar at 0445 UT overlain onto a swath of the 135.6-nm aurora obtained from SSUSI onboard the DMSP Fight 18 are shown in Figure 7. Figure 7a shows the observation from the Jiamusi radar at 0445 UT overlay on the swath of auroral image; Figure 7b shows observation from the Hokkaido East radar at the same time overlay on the swath of auroral image; to check if the two radars observed the same flows, we superimpose the observations from the two radars together with the auroral image and show them in Figure 7c. Each panel is present in MLAT-MLT format. MLT means magnetic local time. The auroral brightness and the LOS velocity are color coded according to the color bars at the right, respectively. The times

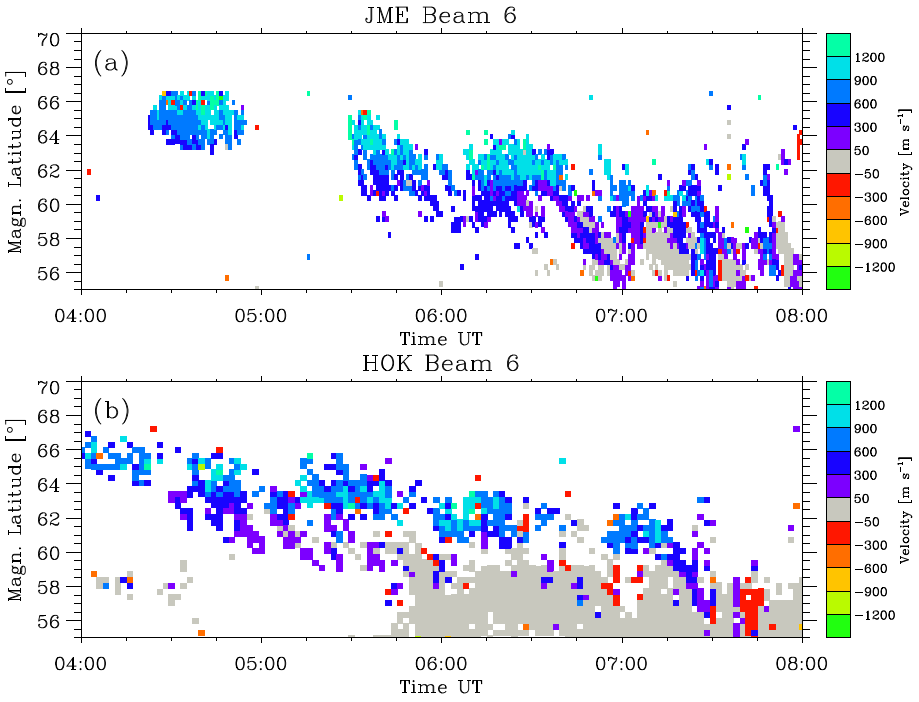

Figure 6. The time series plots of observations from the Beam 6 of the Jiamusi radar (a) and the Hokkaido East radar (b) between 0400 and 0800 UT on 26 August 2018. The LOS velocities are color coded according to the color bar on the right; the ground scatters are marked gray.

of the satellite track are marked in Figure 7b. The figure indicates that the high-velocity westward flows observed on most beams of the two radars are located in the auroral region, so they should be the sunward return flows along the dusk flank rather than subauroral polarization streams. From Figure 7c, we can see that the westward flows observed by the two radars are the same flows. Due to the directions of the beams of the Jiamusi radar are more eastward from the magnetic north than that of the Hokkaido East radar, the LOS velocities observed by the Jiamusi radar are higher than the Hokkaido East radar.

Figure 8 is in the same format as Figure 7 with the radar observation obtained at 0725 UT. The swath of auroral image obtained from SSUSI onboard the DMSP Fight 17 are used in this figure, and the times of the satellite track are marked in Figure 8b. At this moment, an obvious expansion of aurora can be seen with the equatorward edge extended to approximately 53° MLAT. Compared with Figure 7, the expansion of the

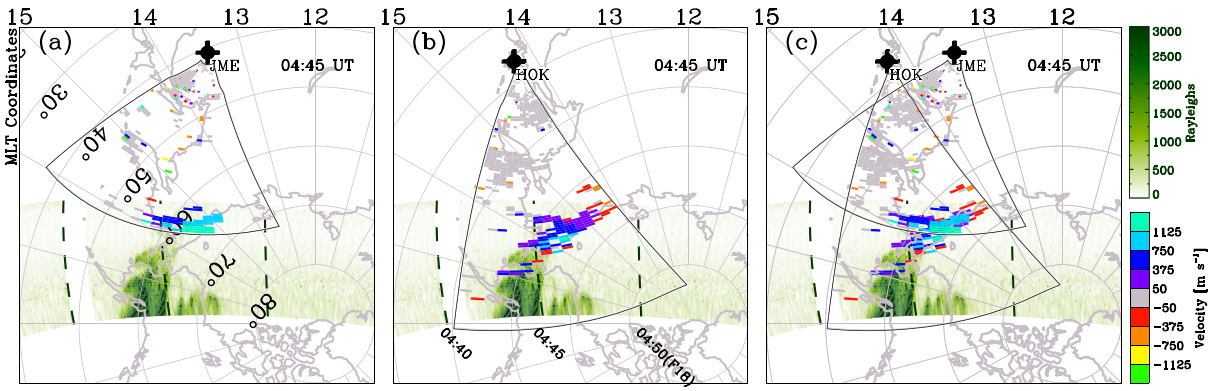

Figure 7. The westward flows observed by the Jiamusi radar and the Hokkaido East radar at 0445 UT overlay onto a swath of the 135.6-nm aurora obtained from SSUSI onboard the DMSP Fight 18. (a) The Jiamusi observation overlay onto the auroral image, (b) the Hokkaido East observation overlay onto the auroral image, and (c) both of the Jiamusi and the Hokkaido East radar observations overlay onto the auroral image. Each panel is present in MLAT-MLT format. The auroral brightness and the LOS velocity are color coded according to the color bars at the right, respectively. The times of the satellite track are marked in Figure 7b.

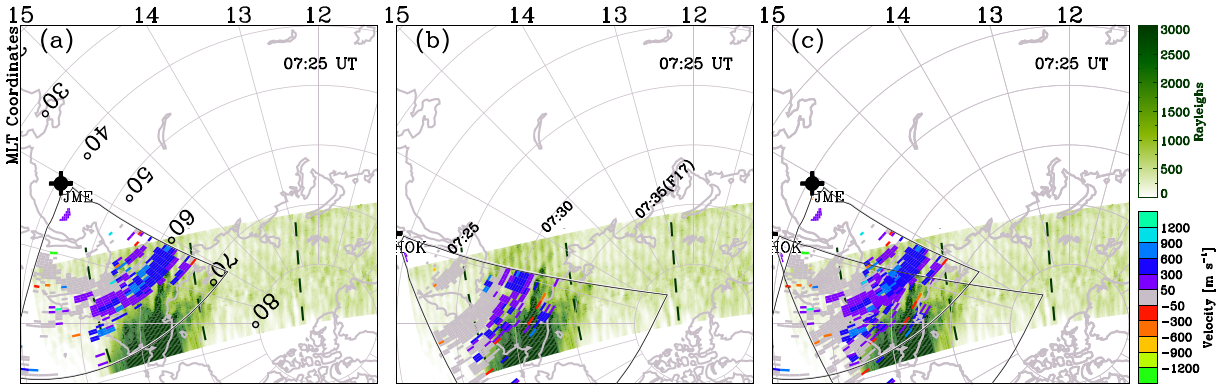

Figure 8. The westward flows observed by the Jiamusi radar and the Hokkaido East radar at 0725 UT overlay onto a swath of the 135.6-nm aurora obtained from SSUSI onboard the DMSP Fight 17 (same format as Figure 7).

scope of the westward flows measured by the two radars was also evident. Another difference from Figure 7 is that the LOS velocities observed by the two radars on 0725 UT were weaker than those observed on 0445 UT. The weaker LOS velocities at 0725 UT can be attributed to the reduced dayside reconnection rate for the southward IMF B_z slightly reduced from 16 nT at 0445 UT to 15 nT at 0725 UT, and velocity of the solar wind reduced from 402 km/s at 0445 UT to 373 km/s at 0725 UT. Besides, the solar wind dynamic pressure can also influence the convection intensity, the work by Boudouridis et al. (2005) indicated that increased solar wind dynamic pressure during southward IMF orientation can enhance the convection intensity. The dynamic pressure of solar wind was 7.71 nPa at 0445 UT, while that was 5.56 nPa around 0725 UT. This can be another factor that accounted for the stronger LOS velocities observed at 0445 UT. Similar with Figure 7, Figure 8 shows that the westward flows observed on most beams of the two radars were located in the auroral region and what the two radars observed were the same westward flows. The figures also demonstrated that the joint measurements by the Jiamusi radar and the Hokkaido East radar can provide two-dimensional measurements for ionospheric convection in the common viewing area.

3.3. Ionospheric Convection Pattern

The SuperDARN was designed primarily for continuous, instantaneous, global-scale ionospheric convection observation. To obtain full two-dimensional velocity vectors, SuperDARN radars operating in pairs with common volume areas to measure the LOS velocities of the ionospheric convection from different facing directions. Ruohoniemi and Baker (1998) developed the analysis procedure to yield the maps of instantaneous ionospheric convection by combining all available SuperDARN Doppler data with a hemisphere. The procedure was further developed by Shepherd and Ruohoniemi (2000). They improved the equatorward

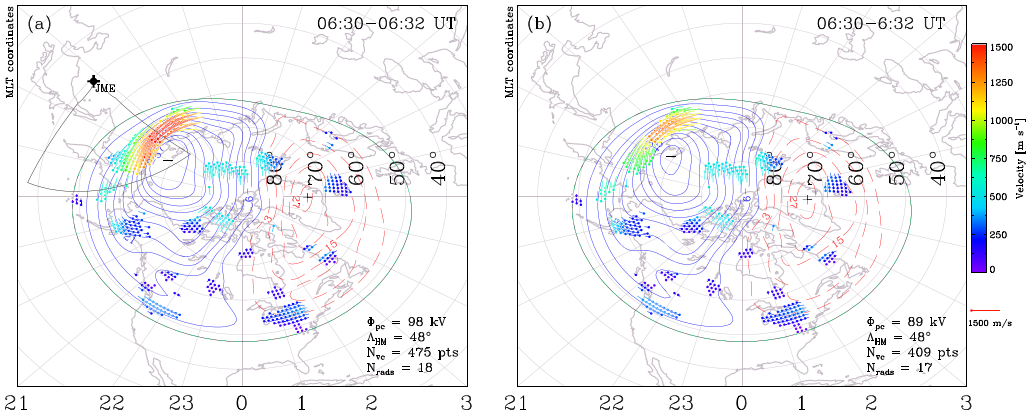

Figure 9. (a) The convection pattern calculated using data from all Northern Hemisphere SuperDARN radars and the Jiamusi radar and (b) the pattern calculated when the Jiamusi data are excluded. Each of the convection patterns is presented in MLAT-MLT format. Contours of electrostatic equipotential are plotted with a contour spacing of 6 kV. The intensity of the fitted velocity vectors is represented by both the length of the vector and the color in the color bar on the right.

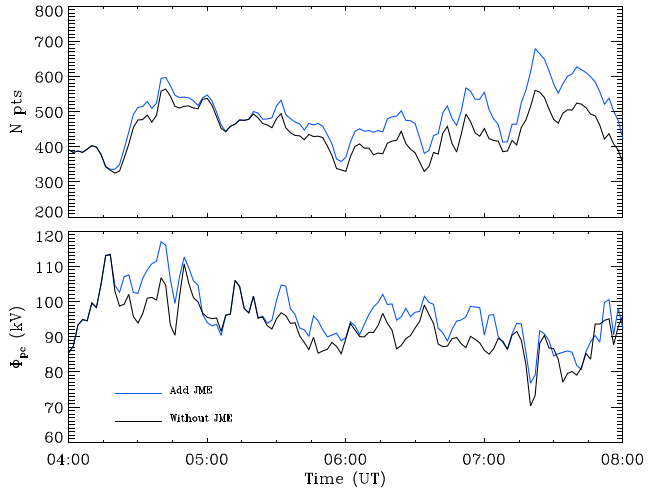

Figure 10. The time series plots of the number of gridded LOS velocity measurements in the calculation of convection (upper panel) and the time series plots of the cross-polar cap potential (lower panel) with (blue curves) and without (black curves) the Jiamusi data between 0400 to 0800 UT on 26 August 2018.

boundary of the convection zone at which the potential is set to 0 by using the MLT and geomagnetic activity dependent Hepper-Maynard (HM) boundary (Heppner & Maynard, 1987). In the previous procedure, the convection boundary is taken to be a circle of constant invariant latitude. Another improvement was the usage of the weighting scheme that reduced the tendency for the statistical model data to dominate the global solution of the cross-polar cap potential at higher-order fittings. Generally, the mapping procedures are as follows now. First, the LOS velocities measured from all available radars are filtered and binned onto a uniform spatial grid. In the second step, the HM boundary is introduced to. In the third step, data from a convection model are used to fill the regions of poor data coverage. The last step is a mathematical fitting procedures to obtain the ionospheric electrostatic potential. For more detailed steps of the procedure please see the references (Ruohoniemi & Baker, 1998; Shepherd & Ruohoniemi, 2000). In this work, the latest version of the radar software toolkit (RST 4.3) of SuperDARN was run to produce the map potential output. In the procedure, the statistical ionospheric convection pattern of Thomas and Shepherd (2018) is used to estimate the ionospheric velocities in regions of poor data coverage. The procedure produces one convection map every 2 min.

In this section, we investigate the effect the Jiamusi radar data had on the calculation of the SuperDARN convection patterns during the main phase of the storm on 26 August 2018. As Baker et al. (2007) did, we calculate the convection patterns including and excluding the Jiamusi data and examine the difference. Figure 9 shows such an example at 0630–0632 UT. The convection pattern calculated using data from all Northern Hemisphere SuperDARN radars and the Jiamusi radar is shown in Figure 9a, and the pattern calculated when the Jiamusi data are excluded is shown in Figure 9b. Each of the convection patterns is presented in MLAT-MLT format. Contours of electrostatic equipotential are plotted with a contour spacing of 6 kV. The fitted velocity vectors are also plotted, the intensity of the fitted velocity vectors is represented by both the length of the vector and the color according to the color bar on the right. The green dotted contour is the HM boundary. The cross-polar cap potential Φ_{pc}, the latitude of the lower limit of the HM boundary (Λ_{HM}), the number of the gridded LOS velocity measurements (N_{vc}), and the number of radars (N_{radars}), which provided the gridded LOS velocity measurements, are given at the lower right of each pattern. The FOV of the Jiamusi radar is plotted in Figure 9a, the radar located in the dusk sector at this time. By comparing the two patterns, it can be seen that the convection in the duskside cell was enhanced by adding the Jiamusi data in the calculation of the convection patterns. The cross-polar cap potential for the pattern in Figure 9a is higher than that in Figure 9b (98 kV vs. 89 kV). This increased polar cross-polar potential for the pattern in Figure 9a can be attributed to the stronger flows measured by the Jiamusi radar and the increase in the number of high-velocity measurements. The number of gridded LOS velocity measurements N_{vc} increases from 409 in Figure 9b to 475 in Figure 9a.

The cross-polar cap potential is a representation of the global convection strength. It is used to give a quantitative measurement of the influence that the Jiamusi data on the convection patterns. Figure 10 shows the time series plots of the variations of number for the gridded LOS velocity measurements in the calculation of convection (upper panel) and cross-polar cap potential (lower panel) between 0400 and 0800 UT. The black curves indicate the variations of the two parameters when the Jiamusi data were excluded from the calculation, while blue curves indicate when the Jiamusi data were included into the calculation. It can be seen that both the number of the gridded LOS velocity measurements and the cross-polar cap potential increased by adding the Jiamusi data into the calculation. According to calculations, the inclusion of the Jiamusi data can increase the number of gridded LOS velocity measurements by up to 24.42%; the cross-polar cap potential can be increased by up to 13.90%. The number of gridded LOS velocity measurements increased by 10.78% on average during the investigated period. The cross-polar cap potential increased by 4.07% on average.

4. Summary and Conclusion

A new middle-latitude HF radar (the Jiamusi radar) was built in China and is currently in full operation. The primary purpose of this paper is to present the first observation of ionospheric convection from the radar

during a strong geomagnetic storm and show the application of the data in calculating the global-scale convection pattern during strong geomagnetic activity. During the main phase of the storm which occurred on 26 August 2018, the radar measured very strong westward flows with a maximum LOS velocity that exceeded 1,000 m/s and the radar captured the equatorward movement feature of the flows. The measurements have been compared with the simultaneous measurements from the SuperDARN Hokkaido East radar. The results demonstrated that the two radars observed the same westward flows in the common volume area during that period and the features of westward flows including the equatorward expansion and tendency of variation of the LOS velocities observed by the two radars were consistent with each other. Joint analysis by combining the auroral observation and radar measurements indicated that the high-velocity westward flows observed by the two radars are sunward return flows of the duskside convection cell. We also examined the impact of including the Jiamusi data in the calculation of the Northern Hemisphere convection patterns during the storm main phase by comparing convection patterns calculated with and without the Jiamusi data. During the investigated period, the inclusion of the Jiamusi data can increase the cross-polar cap potential by up to 13.90%. In conclusion, the Jiamusi radar data have been proved valid, and they can improve the global-scale convection pattern by providing more measurements to the convection calculation procedure during a strong storm event.

Acknowledgments
Construction of the Jiamusi radar was made possible by fund provided by the National High-tech Research and Development Program of China. This work was supported by NNSFC Grants 41774155, 41731070, and 41574159 and by the Strategic Pioneer Program on Space Science, Chinese Academy of Sciences, Grant XDA15052500 and was supported in part by the Specialized Research Fund for State Key Laboratories of China. It was also supported by Key Research Program of Frontier Science, Chinese Academy of Sciences, Grant QYZDJ-SSW-JSC028. The author J. J. Zhang was also supported by the Young Elite Scientists Sponsorship Program by Chinese Association for Science and Technology. The authors acknowledge the use of SuperDARN data and SSUSI data. SuperDARN is a collection of radars funded by national scientific funding agencies of Australia, Canada, China, France, Italy, Japan, Norway, South Africa, United Kingdom, and the United States; data can be accessed via this website (http://vt.superdarn.org/tiki-index.php?page=Data+Access). The fitacf data of the Jiamusi radar from 0400 to 0800 UT on 26 August 2018 are available at Zenodo (https://doi.org/10.5281/zenodo.3526986). The SuperDARN radar software toolkit (RST) 4.3 is available at Zenodo (https://doi.org/10.5281/zenodo.3401622). The data visualization toolkit developed by the SuperDARN group of Virginia Tech can be downloaded from this site (https://github.com/vtsuperdarn/davitpy). The SSUSI auroral energy flux data are available at this site (http://ssusi.jhuapl.edu/). Our acknowledgment also goes to CDAWeb of the Goddard Space Flight Center for use of the solar wind data and SYM-H index from OMNI database.

References

Axford, W. I., & Hines, C. O. (1961). A unifying theory of high-latitude geophysical phenomena. *Canadian Journal of Physics*, *39*, 1433–1464.

Baker, J., Greenwald, R., Ruohoniemi, J., Oksavik, K., Gjerloev, J., Paxton, L., & Hairston, M. (2007). Observations of ionospheric convection from the Wallops SuperDARN radar at middle latitudes. *Journal of Geophysical Research*, *112*, A01303. https://doi.org/10.1029/2006JA011982

Boudouridis, A., Zesta, E., Lyons, L. R., Anderson, P. C., & Lummerzheim, D. (2005). Enhanced solar wind geoeffectiveness after a sudden increase in dynamic pressure during southward IMF orientation. *Journal of Geophysical Research*, *110*, A05214. https://doi.org/10.1029/2004JA010704

Chen, C., Liu, Y. D., Wang, R., Zhao, X., Hu, H., & Zhu, B. (2019). Characteristics of a gradual filament eruption and subsequent CME propagation in relation to a strong geomagnetic storm. *The Astrophysical Journal*, *884*(1), 90. https://doi.org/10.3847/1538-4357/ab3f36

Chisham, G., Lester, M., Milan, S. E., Freeman, M. P., Bristow, W. A., Grocott, A., et al. (2007). A decade of the Super Dual Auroral Radar Network (SuperDARN): Scientific achievements, new techniques and future directions. *Surveys in Geophysics*, *28*(1), 33–109.

Crooker, N. U. (1992). Reverse convection. *Journal of Geophysical Research*, *97*(A12), 19,363–19,372. https://doi.org/10.1029/92JA01532

Dungey, J. W. (1961). Interplanetary magnetic field and the auroral zones. *Physical Review Letters*, *6*, 47–48.

Foster, J. C. (1983). An empirical electric field model derived from chatanika radar data. *Journal of Geophysical Research*, *88*(A2), 981–987.

Friis-Christensen, E., Kamide, Y., Richmond, A., & Matsushita, S. (1985). Interplanetary magnetic field control of high-latitude electric fields and currents determined from greenland magnetometer data. *Journal of Geophysical Research*, *90*(A2), 1325–1338.

Heppner, J., & Maynard, N. (1987). Empirical high-latitude electric field models. *Journal of Geophysical Research*, *92*(A5), 4467–4489.

Kivelson, M. G., & Russell, C. T. (1995). *Introduction to Space Physics*. New York, USA: Cambridge University Press.

Nishitani, N., Ruohoniemi, J. M., Lester, M., Baker, J. B. H., Koustov, A. V., Shepherd, S. G., et al. (2019). Review of the accomplishments of mid-latitude Super Dual Auroral Radar Network (SuperDARN) HF radars. *Progress in Earth and Planetary Science*, *6*(1), 27. https://doi.org/10.1186/s40645-019-0270-5

Pettigrew, E. D., Shepherd, S. G., & Ruohoniemi, J. M. (2010). Climatological patterns of high-latitude convection in the northern and southern hemispheres: Dipole tilt dependencies and interhemispheric comparisons. *Journal of Geophysical Research*, *115*, A07305. https://doi.org/10.1029/2009JA014956

Rich, F. J., & Hairston, M. (1994). Large-scale convection patterns observed by DMSP. *Jornal of Geophysical Research*, *99*(A3), 3827–3844.

Richmond, A. D., & Kamide, Y. (1988). Mapping electrodynamic features of the high-latitude ionosphere from localized observations-Technique. *Journal of Geophysical Research*, *93*(A6), 5741–5759.

Ruohoniemi, J. M., & Baker, K. B. (1998). Large-scale imaging of high-latitude convection with Super Dual Auroral Radar Network HF radar observations. *Journal of Geophysical Research*, *103*(A9), 20,797–20,811.

Ruohoniemi, J. M., & Greenwald, R. A. (1996). Statistical patterns of high-latitude convection obtained from Goose Bay HF radar observations. *Journal of Geophysical Research*, *101*(A10), 21,743–21,763.

Ruohoniemi, J. M., & Greenwald, R. A. (2005). Dependencies of high-latitude plasma convection: Consideration of interplanetary magnetic field, seasonal, and universal time factors in statistical patterns. *Journal of Geophysical Research*, *110*, A09204. https://doi.org/10.1029/2004JA010815

Shepherd, S. G., & Ruohoniemi, J. M. (2000). Electrostatic potential patterns in the high-latitude ionosphere constrained by SuperDARN measurements. *Journal of Geophysical Research*, *105*(A10), 23,005–23,014. https://doi.org/10.1029/2000JA000171

Sotirelis, T., Korth, H., Hsieh, S.-Y., Zhang, Y., Morrison, D., & Paxton, L. (2013). Empirical relationship between electron precipitation and far-ultraviolet auroral emissions from DMSP observations. *Journal of Geophysical Research*, *118*, 1203–1209. https://doi.org/10.1002/jgra.50157

Sterne, K. T., Greenwald, R. A., Baker, J. B. H., & Ruohoniemi, J. M. (2011). Modeling of a twin terminated folded dipole antenna for the Super Dual Auroral Radar Network (SuperDARN). In *Radar Conference*. Kansas City, MO, USA: IEEE. https://doi.org/10.1109/RADAR.2011.5960673

Thomas, E. G., & Shepherd, S. G. (2018). Statistical patterns of ionospheric convection derived from mid-latitude, high-latitude, and polar SuperDARN HF radar observations. *Journal of Geophysical Research*, *123*, 3196–3216. https://doi.org/10.1002/2018JA025280

Weimer, D. (1996). A flexible, IMF dependent model of high-latitude electric potentials having "space weather" applications. *Geophysical Research Letters*, *23*(18), 2549–2552.

Weimer, D. R. (1995). Models of high-latitude electric potentials derived with a least error fit of spherical harmonic coefficients. *Journal of Geophysical Research*, *100*(A10), 19,595–19,607.

Zhang, Q.-H., Zhang, B.-C., Lockwood, M., Hu, H.-Q., Moen, J., Ruohoniemi, J. M., et al. (2013). Direct observations of the evolution of polar cap ionization patches. *Science*, *339*(6127), 1597–1600.